

# Sedapp [v2021](#): a non-linear diffusion-based forward stratigraphic model for shallow marine environments

Jingzhe Li<sup>1,2</sup>, Piyang Liu<sup>3</sup>, Shuyu Sun<sup>4</sup> (✉), Zhifeng Sun<sup>2,1</sup>, Yongzhang Zhou<sup>5</sup>, Liang Gong<sup>6</sup>, Jinliang Zhang<sup>7</sup>, Dongxing Du<sup>1,2</sup>

5

1. College of Electromechanics, Qingdao University of Science and Technology, Qingdao 266061, China
2. Geo-Energy Research Institute, Qingdao University of Science and Technology, Qingdao 266061, China
3. School of Science, Qingdao University of Technology, Qingdao, 266520, China
4. King Abdullah University of Science and Technology, Jeddah 23955-6900, Saudi Arabia
5. School of Earth Science and Geological Engineering, Sun Yat-sen University, Guangzhou 510275, China
6. School of New Energies, China University of Petroleum (EastChina), Qingdao 266555, China
7. Department of Geography, Beijing Normal University, Beijing 100875, China

10

Correspondence to: Shuyu Sun (frank.sun.sa@gmail.com)

## Abstract

15

The formation of stratigraphy in shallow marine environments has long been an important topic within the geologic community. Although many advances have been made in the field of forward stratigraphic modelling (FSM), there are still some shortcomings to the existing models. In this work, the authors present our recent development and application of Sedapp: a new non-linear open-source R code for FSM. This code uses an integrated depth-distance related function as the expression of the transport coefficient to underpin the FSM with more along-shore details. In addition to conventional parameters, a negative-feedback sediment supply rate and a differentiated deposition-erosion ratio were also introduced. All parameters were implemented in a non-linear manner. Sedapp is a ~~3D~~(2DH tool that is also capable of running ~~2D~~(1DH scenarios. Two simplified case studies were conducted. The results show that Sedapp can not only assist in geologic interpretation, but is also an efficient tool for internal architecture predictions.

20

25

**Keywords:** Forward stratigraphic modelling, continental shelf, R codes, fluvial-deltaic, continental fault basin

## 1 Introduction

Shallow marine areas are among the most active environments for sedimentation, where sea level, tectonism, climate all influence the interactions between land and sea. The sedimentary successions formed in these areas are an important archive of the past interactions. In addition, the archive itself can be an ideal hydrocarbon accumulation place. From this archive, a large number of theoretical and field studies have made great achievements and accumulated a wealth of data in the past decades.

In order to better interpret the specific processes and analyze the internal architectures, many forward stratigraphic models (FSM) are built in a range of temporal and spatial scales. According to their purposes, these models can be roughly divided into two categories. The first is a full source-to-sink type, which mainly analyzes the deposition and erosion processes from the perspective of the whole sediment chain. In addition to analyzing the depositional response in the downstream unloading area, this kind of model also deals with the precipitation and tectonic uplift in the upstream catchments area, which directly determines the flux of water and sediment (Armitage et al., 2011;2018; Ding et al., 2019; Guerit et al., 2019; Zhang J.Y. et al., 2020). The second, which we choose here, is a sink-dominant type, which focuses on analyzing the architectures and stacking patterns of the sedimentary results in a forward manner (Rivenaes, 1997; Dalman and Weltje, 2012; Li et al., 2020). This type generally does not consider how the sediments in the source area are entrained. Instead, it usually takes the sediment supply rate as a known condition. This kind of model is appropriate for rapid evaluation of the underground strata and prediction of potential hydrocarbon reservoirs by fitting some known evidences, especially in the shallow marine environments.

For long-term processes, sediment flux is usually assumed to be proportional to the topographic gradient. Thus, through the mass conservation law, a diffusion equation like Eq. (1) is generally used in FSM models (Paola, 2000).

$$\frac{\partial h}{\partial t} = \nabla \cdot (\Gamma \nabla h) \tag{1}$$

where  $h$  denotes the topography,  $t$  denotes the time and  $\Gamma$  denotes the transport coefficient. If  $\Gamma$  is a constant or it does not change with the unknowns, these models are usually called linear models. While if  $\Gamma$  changes with the primary unknown  $h$ , these models are called non-linear models.

55 In many cases, linear models are not very competent when the stratigraphic result and its  
controlling factors are interactively connected. For example, the topography evolution in the marine  
portion is seriously affected by the water depth, while the water depth is generally a function of the  
topography and the sea level. In this case, non-linear models seem to be more suitable. Many existing  
60 non-linear models define the transport coefficient using water depth-related functions (e.g., in Clarke et  
al .1983; Kaufman,1991; Syvitski and Hutton, 2001, the coefficient value was assumed to fall  
exponentially with the water depth ). The water depth models could work well in general coastal zones.  
However, in the shallow marine environments with river injection, these models become not so  
effective, especially in reflecting the shoreline shape in plane view. Depositional processes around the  
river mouth are more active than those at a distance, even when they are at the same water depth.

65 Additionally, according to Eq. (1), if  $\Gamma$  is fixed, for a given site, deposition or erosion (i.e.,  $\partial h/t >$   
0 or  $\partial h/ \partial t < 0$  ) seems to depend solely on the topographic gradient. However, in a basin, the  
efficiency of deposition and erosion can be very different, even if the slope, sediment supply, and water  
flux are the same. For example, some bed surface is “hardground”, which is very difficult to be eroded.  
While the overlying deposition process is relatively easy. In this case, the distinction between the two  
70 processes seems necessary. For a long-term stratigraphic forming process, there may exist many  
sedimentary discontinuities, which may provide long enough time to generate a variety of  
“hardgrounds” (e.g. the fractal stratigraphic theory in Miall, 2015, etc.). This is actually a reflection  
of the efficiency ratio of deposition to erosion. This is less involved in the existing FSM models.  
Although some source-to-sink models (e.g. Guerit et al., 2019) have introduced the distinction between  
75 deposition and erosion processes, the complex parameter settings still severely limit its practicability in  
a quick result-fitting.

~~Stratigraphic formation in this environment has long been an important topic within the~~  
~~geoscience community, which has directly resulted in the emergence of sequence stratigraphy (Haq et~~  
~~al., 1987; Li et al., 2015; Catuneanu, 2019). Traditional qualitative methods on this subject have made~~  
80 ~~great advances in the past half century, but it is difficult to test the validity and internal consistency of a~~  
~~new concept and are less likely to raise counter-intuitive ideas which may actually be true (Burgess,~~  
~~2012; Burgess and Prince, 2015).~~

~~Computer modelling can help resolve this problem. The methodology is usually called forward~~  
~~stratigraphic modelling (FSM) (Griffiths and Hadler-Jacobsen, 1995; Dalman and Weltje, 2012;~~

85 Sangster et al., 2019), although it was also called stratigraphic forward modelling (Burgess, 2006; Saechi et al., 2015; 2016; Ding et al., 2019), basin filling modelling (Syvitski and Hutton, 2001; Hutton and Syvitski, 2008; Li et al., 2020), and stratigraphic simulation (Rivenaes, 1992; 1997; Lawrence et al., 1990), etc.

90 FSM deals mainly with long-term geomorphologic/stratigraphic dynamics (Paola, 2000). It is slightly different from sediment fluid-flow models, which deal more with the fluid-flow dynamics by solving modified Navier-Stokes equations within a full study domain (generally shallow water equations, e.g. HydroSedFoam of Zhu et al., 2019 or Delft3D in Ramos et al., 2019). FSM models can be classified into two types, i.e. rule-based models (based on geometric or fuzzy logic) and equation-based models (Paola, 2000; Syvitski and Hutton, 2001; Burgess et al., 2012; Saechi et al., 95 2015). The first type easily captures essential features and is less time-intensive, while it does a relatively poor job of demonstrating predictability and revealing the physical processes (Strobel et al., 1989; Kendall et al., 1991; Burgess, 2012). The latter type is also known as deductive models, which are process-based and solve governing equations (Kaufman et al., 1991; Rivenaes, 1992; Granjeon and Joseph, 1999; Griffiths et al., 2001; Hutton and Syvitski, 2008; Li et al., 2020). For these long-term 100 processes, sediment flux is usually assumed to be proportional to the topographic gradient. Thus, a diffusion equation like Eq. (1) is generally used to derive the governing equations in FSM models (Salles et al., 2018; Ding et al., 2019).

$$\frac{\partial h}{\partial t} = \nabla \cdot (\Gamma \nabla h) \quad (1)$$

where  $h$  denotes the topography,  $t$  denotes the time and  $\Gamma$  denotes the transport coefficient.

105 Diffusion-based models are good at modeling scaled stratigraphic sequence (relative larger scales, e.g. clinoform formation) processes.  $\Gamma$  in Eq. (1) can be defined using different values for different environments (Zhang et al., 2020). Various  $\Gamma$  types are used based on different needs and environments (Rivenaes, 1997; Zhang et al., 2020). Models with constant  $\Gamma$  values are usually called linear models; otherwise, they are known as non-linear models.

110 Although the sediment diffusion assumption is considered a practical representation of long-term slope processes, it is still too simplistic when the  $\Gamma$  is used as a constant because natural agents such as air and water, phenomena such as mass wasting, and biological agents actually move sediment at rates that are not determined solely by slope (Salles et al., 2018). This severely limits the application scope

of linear diffusion-based models. On the contrary, non-linear models are relatively more flexible. Many non-linear models define the transport coefficient using water depth-related functions (e.g., Clarke et al. 1983; Kaufman, 1991). These water depth models work well in general coastal zones. However, in the shallow marine environments with river injection, the water depth models are usually not applicable. Depositional processes around the river mouth are more active than those at a distance, even when they are at the same water depth. Hence, it is difficult for water depth models to reveal along-shore variability, especially in 3D scenarios (actually 2D-H, with two horizontal dimensions and the elevation H). Because of this reason, many hybrid hydrodynamic-diffusion models were proposed. For example, river plume was introduced to differentiate the suspended sediment fluxes along the coastline (Syvitski and Hutton, 2001; Hutton and Syvitski, 2008; Dalman and Weltje., 2012). This treatment realized the modelling of the convex shapes of delta out from the river mouths. However, the computational load was also significantly increased because of the newly added advection-diffusion process. The introduction of many hydrodynamic parameters also increased the difficulty of its usage.

In addition, many existing models are not free or open-source, making it difficult for people to reproduce and improve them. Some codes, although free, can only be used in Linux systems, which makes them inconvenient to use in most PC terminals.

In this paper, we propose a new non-linear FSM model, which is expected to overcome the shortcomings of the existing models. Along with some other features, this model is integrated into a framework called Sedapp, which is an open-source and cross-platform application written in R. We use examples to show how this model works and test its effectiveness and convenience in reconstruction of sedimentary systems, revealing their internal architectures.

## 2 Methodology

### 2.1 Mathematical model

The Sedapp mathematical model can be expressed as follows:

$$F_i \frac{\partial h}{\partial t} = \max \left( \nabla \cdot (\Gamma_i \nabla h), \frac{1}{Der} \nabla \cdot (\Gamma_i \nabla h) \right) + q \quad (2)$$

$$\sum_i^n F_i = 1 \quad (3)$$

140 where  $F_i$  is the fraction of the  $i$ th class of lithology,  $h$  is elevation,  $t$  is time,  $\nabla$  is the nabla operator,  $Der$  is a user-defined parameter denoting the ratio of deposition to erosion (it can be a scalar, vector or tensor value depending on its temporal and spatial variability),  $\Gamma_i$  is the diffusion coefficient for the  $i$ th class of lithology, and  $q$  is the source term that is a function of coordinates and time (the source term is used only for endogenetic sedimentation, especially carbonates. If endogenetic sedimentation is  
145 ignored, the source term can be left out). Among them,  $h$  and  $F_i$  are the primary unknowns.

Note that  $\Gamma_i$  cannot be outside the parentheses, because they are not constants but rather functions of spatial coordinates and time. The expression of a general  $\Gamma$  can be expressed as:

$$\Gamma = \max\left(\alpha e^{-\frac{D(x,h,sl)^\eta}{\beta}}, \alpha_{wd} e^{-\frac{Wd(x,h,sl)^{\eta_{wd}}}{\beta_{wd}}}\right) + \varepsilon \quad (4)$$

where  $\alpha/\alpha_{wd}$  are preexponential factors ( $L^2/T$ ),  $\eta/\eta_{wd}$  are distance indexes (no dimension),  $\beta/\beta_{wd}$  are  
150 spatial scale factors ( $L^\eta$  or  $L^{\eta_{wd}}$ ), and  $\varepsilon$  is an adjustment factor ( $L^2/T$ ) reflecting the environment energy. In particular, distance function  $D=D(x, \#h, \#sl)$  and water depth function  $Wd(x, \#h, \#sl)$  change with spatial coordinates [x](#), [topography h](#) and [time the sea level sl](#), and they work for the marine portion only.

When  $Der = 1$  and  $n = 2$ , the 3D (actually 2DH, because  $h$  is another dimension perpendicular to  $x$  and  $y$ ) scenario for Eq. (2) and Eq. (3) can also be expressed as:

$$155 \quad F \frac{\partial h}{\partial t} = \frac{\partial}{\partial x} \left( \Gamma_1 \frac{\partial h}{\partial x} \right) + \frac{\partial}{\partial y} \left( \Gamma_1 \frac{\partial h}{\partial y} \right) + q(x, y, t) \quad (5)$$

$$(1 - F) \frac{\partial h}{\partial t} = \frac{\partial}{\partial x} \left( \Gamma_2 \frac{\partial h}{\partial x} \right) + \frac{\partial}{\partial y} \left( \Gamma_2 \frac{\partial h}{\partial y} \right) + q(x, y, t) \quad (6)$$

where  $x$  and  $y$  are spatial coordinates. This is especially suitable for cases dealing only with two classes of lithology for simplicity, where  $\Gamma_1$  is the transport coefficient for sand and  $\Gamma_2$  is the transport coefficient for mud.

160 For 2D (1D-H) scenarios, especially along the section line through the river mouth, the distance related term is generally larger than the water depth related term, so the latter term within the max function in Eq. (4) is usually omitted. For convenience in coding, also ignoring the endogenetic sedimentation, Eq. (5), Eq. (6) and Eq. (4) can be simplified into:

$$F \frac{\partial h}{\partial t} = \frac{\partial}{\partial x} \left( \Gamma_1 \frac{\partial h}{\partial x} \right) \quad (7)$$

165

$$(1 - F) \frac{\partial h}{\partial t} = \frac{\partial}{\partial x} \left( \Gamma_2 \frac{\partial h}{\partial x} \right) \quad (8)$$

$$\Gamma_i = \alpha_i \cdot e^{-\frac{(c \cdot D(x,t))^2}{E}} + \varepsilon, i = 1, 2 \quad (9)$$

170

The joint effect of  $c$  and  $E$  in Eq. (9) is equivalent to that of  $\beta$  in Eq. (4). The variable  $c$  here, with a dimension of  $L^{-1}$ , is mainly used to facilitate the scale of distance and differentiate the transport characteristics of different sediment types (e.g., sand and mud).  $E$  is a dimensionless constant that represents hydraulic characteristic energy.

## 2.2 Code Implementation

175

Sedapp was written in the R language and its solution procedure was based on the finite volume method (FVM), which has the desired property of local mass conservation and has a clear physical meaning (Versteeg and Malalasekera, 2007; Moukalled et al., 2016; Liu P. et al., 2017). The cell-centered variable arrangement method was used to store the unknowns at the grid element centroids. The non-linearity was implemented through stepwise iteration (Fig.1).

The brief work-flow within a single time step is as below:

180

- 1) Implement user-defined tectonic subsidence and update the topography;
- 2) Implement user-defined sea level and identify/update the shoreline location;
- 3) Solve the differential deposition/erosion function;
- 4) Implement the compaction and isostatic subsidence.

185

Step 3) is a major step. According to the hypothesis of diffusion-based FSM models, the change rate (by either deposition or erosion) is proportional to the gradient of the slope (Fernandes et al., 1997; Pelletier, 2013). If we use the diffusion equation/law directly without any differential treatments between deposition and erosion (in other words, Der is held at 1), it will be very difficult to treat some complex situations. For example, some bed surface is “hardground”, which is very difficult to be eroded, while the overlying deposition process is relatively easy—contrary to the geological knowledge that deposition and erosion processes are two distinct processes with different rates. Hence, for a given location, the erosion and deposition could occur at different rates~~the max() function is used as in Eq-~~ (2). Generally, ~~the erosion process occurs at a different rate than deposition (also called erosion constraints, see Galy and France-Lanord, 2001), so and~~ Der ~~is usually~~ could be set not be equal to 1. For example, if we wanted the erosion rate to be only 1/100 of the deposition rate, the Der can be set to 100.

190

Through the  $\max()$  function in Eq. (2) ~~In this case, if it is for~~ a deposition process (namely the  $\frac{\partial h}{\partial t} > 0$ ),

195  $\nabla \cdot (\Gamma_i \nabla h)$  would be larger than  $\frac{1}{der} \nabla \cdot (\Gamma_i \nabla h)$ , and  $\nabla \cdot (\Gamma_i \nabla h)$  is used. Otherwise, the  $\frac{1}{der} \nabla \cdot (\Gamma_i \nabla h)$  is used. If a non-erosion case is desired, Der can be set to a very large value.

Generally, sediment supply rate cannot be directly defined through boundary condition settings, since the latter can only determine the boundary slope. Therefore, Sedapp uses a negative-feedback strategy to define the sediment supply rate. At each time step, the total amount of deposition within a step is first calculated using the previously defined  $\alpha_{test}$ , and then the adjusted  $\alpha_{mod}$  is calculated by

200 Eq. (10):

$$\alpha_{mod} = \alpha_{test} \frac{V_{expected}}{V_{test}} \quad (10)$$

where  $\alpha_{mod}$  denotes the modified  $\alpha$  of this time step;  $V_{expected}$  denotes the expected sediment increment, namely the sediment supply rate; and  $V_{test}$  denotes the computed sediment increment with  $\alpha_{test}$ .

### 3 Characteristics

#### 205 3.1 Nonlinear transport coefficients

The nonlinear transport coefficient is a feature of Sedapp. Sedapp's transport coefficient uses a function of both the distance from the estuary and the water depth. This feature makes it easier to simulate fluvial-deltaic processes in [32DH](#) scenarios, which can reflect changes along the shore. Even in [2D1DH](#) cases, this feature also has some advantages (see the discussion section for details).

210 Generally, a smaller  $c$  value results in higher sediment travel distance and a larger distribution range when the total amount of sediment is fixed. For example, the  $c$  of mud is usually set to 50%-85% of sand, thus reflecting the differential deposition of sand and mud. In addition, the environment energy  $\mathcal{E}$  can also influence the sediment travel distance that a larger  $\mathcal{E}$  can make the sediment travel further. As sedimentation progresses, the position of the estuary may change, so the distance from the estuary is  
215 updated at each time step to achieve the nonlinearity of  $\Gamma$ .

#### 3.2 Differential and customizable deposition/erosion rate

During the actual deposition process, the properties of the lower strata (such as compaction



degree, lithology, and age, etc.), as well as some external environmental factors (such as temperature, humidity and pH value, etc.), will affect the erosion rate. Therefore, the customized treatment of erosion rate is another Sedapp characteristic.

In Sedapp, the deposition rate is a parameter that can be specified directly (for the adjustment process see section 2.2). Furthermore, the Der parameter is a user-defined parameter that controls the ratio of deposition rate to erosion rate. When Der is 1, the deposition rate is equal to the denudation rate (Fig.2a), and when Der value is 10 or 100, denudation is significantly weakened (Fig.2b). Theoretically, if the value of Der is large enough, it is equivalent to completely eliminating the denudation effect. Der values should be customized according to the actual situation.

### **3.3 Customizable compaction**

Compaction is an important geological process after sediment deposition, especially when the sediment thickness is very high. In Sedapp, the compaction process can be easily realized by setting the composition of lithology and porosity curves.

In this paper, we designed a pyramid-shaped mountain simulation commonly used by other researchers (as shown in Fig.3, see Rivenaes,1992 and Yuan et al.,2019 for reference). The Der value was set to 1. The sediment supply ratio of sand and mud was set to 1:1, and the porosity curve was set as shown in Fig.3d. After simulation, the top of the pyramid was denuded and the foot of the pyramid had deposited sediment of a given thickness.

To illustrate the effect of compaction, Sedapp introduces a scale factor that can enlarge the longitudinal scale. Fig.3a shows the original compression scale (that is, the scale factor was equal to 1), and the scale factors in Fig.3b and Fig.3c were 100 and 1000, respectively. It can be seen that sediment thickness at the foot of the pyramid in Fig.3c was significantly smaller than that in Fig.3a. The factors that caused these differences were not only depth but also the proportion of sand and mudstone and the shape of depth-porosity curves, which can be easily adapted to different scenarios by modifying the lithologic proportion and porosity-depth functions in Sedapp.

## **4 Verification of Sedapp**

To identify how well the algorithm works within geological context, some simple benchmark simulations are given below.

#### 4.1 Typical stacking patterns

Typical stacking patterns including forced regression, normal regression, and transgression can be formed (Fig.4) by fixing sediment supply while controlling the adjusted sea level rise rate.

250 During the period of sea-level decline, the shoreline moved seaward, and the onlap points also moved seaward and form the offlap and downlap stratigraphic termination structures (Fig.4a). During slow sea-level rise, the shoreline continued to move seaward, but the onlap points started to move landward, forming an onlap termination structure. At the other end, the downlap structure continued to exist. During rapid sea-level rise, the shoreline started to move landward and the onlap points also moved landward. At this time, downlap structure did not exist above the slope break, but may have  
255 existed below the slope break.

#### 4.2 Typical two-cycle scenario

To demonstrate the complete base level changing process, this paper designed a simulation with two full sinusoidal cycles as shown in Fig.5. In the first cycle, the shoreline dropped and moved seaward. Then it slowly rose and gradually moved landward until it reached the highest point and  
260 tended to stabilize. The water depth of deposition in the strata gradually deepened from left to right on the marine side (Fig.5a), and the sandy content reached a maximum around the shoreline (Fig.5b) near the shoreline. In the strata on the land side, the sand content was stratified. The sand content was relatively large during the early transgression and subsequently relatively small. The second cycle was located above the first cycle and continued the same characteristics as the first cycle, but the deposition  
265 range was enlarged and the average single layer thickness was thinner.

#### 4.3 Case studies

##### 1) Model 1

In order to better display the [3D2DH](#) performance of Sedapp, this paper designed a model called Model 1. Its length and width ranges were both 200m, and the elevation range was about 10m. The  
270 mesh was  $200 \times 200$  in x-y plane. The time span of the model was set at 10 Ma, and the step size was set at 0.5 Ma. Sea level was kept constant at 3 m. Its initial topography was set as that in Fig.6a. A river was set up in the central position of y-axis ( $y = 100\text{m}$ ). The channel shape of the river was set in advance being a sine curve. Fluvial profile slope is set to a constant of 0.00357, while the sediment

supply rate was not defined since it could vary according to the fluvial profile slope. The other main parameters of the model are shown in Tab. 1.

The projection of the simulation results on the x-y plane clearly shows the variation characteristics of the along the shore. When  $t = 0$ , the shoreline was a straight line, and the channel was in the middle of the shoreline. As time went on, the river mouth continued to move forward. From 0 to 2 Ma, the channel first swung to the north, then to the south, and shoreline began to bulge slightly towards the sea side. From 2Ma, the channel continued to swing southward, until the time approached 4Ma and the river mouth began to turn north slowly. From 4Ma to 6Ma, the channel continued to swing northward, and the convex part towards the sea side became more and more obvious. From 6Ma to 8Ma, the channel continued the previous trend, while the convex shoreline became asymmetry (an increasing skewness to the north). From 8 Ma to 10 Ma, the principal line of the channel moved southward, and the convex shoreline gradually returned to symmetry (Fig.7).

The simulation results also show some interesting features on longitudinal sections. Two sections ( $y = 75\text{m}$  and  $y = 125\text{m}$ ) perpendicular to the shoreline direction are selected (see Fig.7f for the position of the section line). The two sections are located on the north and south sides of the main channel. The distance between the channel and the two sections is varying. In the southern profile ( $y = 75\text{m}$ ), from 4 Ma to 10 Ma, the isochronous lines of the formation changes from sparse to dense, and then from dense to sparse (i.e., the thickness of a single clinoform changes from thick to thin first and then from thin to thick) (Fig.8). This is completely contrary to that observed in the northern profile ( $y = 125\text{m}$ ). From 4Ma to 10Ma, the isochronous lines first changes from dense to sparse, and then from sparse to dense, reflecting that the deposition rate first increases and then decreases (Fig.9).

Under the parameters shown in Tab. 1, due to the existence of estuaries, shoreline will bulge towards the sea side. A closer distance to the river mouth could result in a higher sedimentation rate and a greater shoreline advancing speed. From 2 Ma, the convex shape of the shoreline towards the sea side became more and more apparent, similar to the morphology of some real-world Deltas (Fig.10).

## 2) Model 2

This code can be applied not only to marginal marine environments but also to the continental fault basins. Taking the 3 + 4 sand groups of the third member of Shahejie Formation in the Gaobei slope belt of Nanpu Sag in Bohai Bay Basin as an example, we conducted a simplified [2D-1DH](#) real case study. The basic geological background is as follows: During the deposition period of this set of

strata, the normal fault tectonic movement in the north of the sag was active, which was the main  
305 controlling factor leading to the increase of accommodation space. At the same time, the terrigenous  
clasts came from the north is sufficient, and the basin was in a balanced state (Li et al., 2018).  
According to the geological background, a simplified reconstruction model (Model 2) was designed,  
which assumed that the subsidence rate of the boundary fault and sediment supply rate is constant,  
neglected the effect of isostasy, and considered the effect of sediment compaction.

310 The simulation results are shown in Fig.11. From the perspective of temporal and spatial  
stratigraphy, the shoreline mainly moved towards the sag center during the early stage, and then moved  
back to the land side. The deepest water depth occurs in the middle south part at 2 Ma (Fig.11a). This  
shoreline phenomenon is usually called autoretreat (Muto and Steel, 2002). The sand fraction section  
shows that the steep slope belt in the north is richer in sand content than the south (Fig.11b). The  
315 porosity section shows that the porosity generally decreases from bottom to top. The porosity also  
varies horizontally, especially when the depth is deeper than 800 m. The porosity in the north is larger  
than that in the south.

Due to the over-simplified assumptions, the simulation results are not necessarily be consistent  
with every practical borehole. However, the general trends are revealed through the simulation, which  
320 can strengthen or improve our existing understanding and guide us to seize the main direction. Also,  
the facies simulation results were in good agreement with the Sedpak results used in Li et al., 2018.

## 5 Discussion

Sedapp is a diffusion-based model, and its transport coefficient is a function of both distance  
from estuary and water depth. Compared with most existing diffusion models based only on water  
325 depth, this modification has great advantages in fluvial-deltaic environments, especially for [3D2DH](#)  
scenarios. Sedapp not only simulates some surface landscapes, but it also reveals some interesting  
internal features. In the sections beside the channel in Model 1, the formation rate of the clinoforms has  
close relationship with the distance between the channel and the section. This may be of great  
significance to the analysis of ancient strata. Considering the resolution of seismic data, it is easier to  
330 observe the changes in the density of the foreset than to directly find a channel. This may provide some  
important supplementary information in areas with less borehole data.

Sedapp also showed strong simulation ability in [2D-1DH](#) scenarios. It is not only competent for the shallow sea environment of continental margin, but also competent for the simulation of continental fault basin (Fig.11). The simulation results have strong comparability with previous studies (Li et al., 2018). In addition, Sedapp can avoid some potential problems that the water depth models may meet. The simulation results of Sedapp and water depth models are not very different where the original slope is gentle (Fig.12a, Fig.12b). However, when the slope is steep, the differences are obvious: due to the steep slope and the sharp increase of water depth, the slope break trajectory simulated by the water depth based model increases significantly, even if the sea level remains unchanged at 6m (Fig.12c). This is seriously ~~contradict to~~[contrary to the common-sensely accepted shoreface profile angle that tends to be a constant as long as the environment doesn't change much \(e.g. Catuneanu, 2006\);- especially in estuary or delta front environments](#). In contrast, Sedapp does not face such a problem. As long as the sea level is constant, the slope break line will remain in a straight line and the clinofolds will also move smoothly to the ocean (Fig.12d).

The transport coefficient is a relatively long-term geomorphologic physical quantity, while wave, tidal, and current energy are relatively short-term hydrodynamic quantities. However, they are closely related. A river entering the sea is a type of jet flow phenomenon. The flow velocity decreases rapidly from the river mouth to the sea, which also has a strong negative correlation with the distance to the mouth of the river. The contour map of water flow velocity is fan-shaped. At the same time, the decrease of velocity is also an important cause of sediment deposition, which also explains the close fan-shaped morphology of a delta front. Correspondingly, an increase in water depth will also decrease the flow velocity. For the open coast without river injection, a model based on water depth seems to be reasonable. However, for a coast with river injection, it is difficult to explain the formation of the fan-shaped morphology of a delta. Therefore, it can be concluded that, in more general cases, the transport coefficient should be a function of short-term water energy, which is related to both the estuary distance and the water depth. When there is river injection, the river process is dominant and the estuary distance function is a reasonable proxy for the transport coefficient. When there is no river injection, the water depth plays the main role. In addition, the particle size is also one of the decisive factors (Nash 1980; Andrews and Bucknam 1987). Hence, a choice function (see Eq. (9)) and differentiated  $\alpha$ 's are used to adapt different environments and lithologies. Although the current results of Sedapp seem plausible, these settings for transport coefficient are still empirical. Due to the complex

nature of the transformation from short-term processes to long-term ones, it is difficult to build an accurate bridge between sediment hydrodynamics and stratigraphic formation, while it may be the focus of the next step.

## 365 **6 Code availability**

The current version of model is available from the project website: <http://zenodo.org/record/41332624556868> or [https://github.com/lijingzheQD/Sedapp\\_v2021](https://github.com/lijingzheQD/Sedapp_v2021) under the Creative Commons Attribution 4.0 International License. The exact version of the model used to produce the results used in this paper is archived on Zenodo. Input data and scripts of the case studies are also presented in this site. For more details about Sedapp, please contact Jingzhe Li via email [lijingzhe@qust.edu.cn](mailto:lijingzhe@qust.edu.cn).

### **Contribution of each author**

JL developed the main algorithm of Sedapp and took the lead in writing the manuscript. PL developed the FVM solver for Sedapp. PL, SS, ZS, YZ, LG, JZ and DD participated in the conceiving of the presented idea. SS supervised the project.

### **Competing interests**

No conflict of interest exists in this manuscript.

### **Acknowledgement**

Financial support was provided by the National Natural Science Foundation of China (42002169), the Initial Fund for Young Scholars of Qingdao University of Science and Technology, and the Research Funding from King Abdullah University of Science and Technology (KAUST) through the grants BAS/1/1351-01. Jingfa Li from Beijing Institute of Petrochemical Technology, Jie Chen from Xi'an Jiaotong University and Hua Zhong from Guangdong University of Finance and Economics also offered constructive advice. [We would also like to thank John Armitage, an anonymous referee, and the GMD editors for their constructive and helpful reviewing and editing work.](#)

## Reference

- Andrews DJ, Bucknam RC. Fitting degradation of shoreline scarps by a nonlinear diffusion model. *Journal of Geophysical Research: Solid Earth*. 1987 Nov 10;92(B12):12857-67.
- 390 [Armitage, J. J., Duller, R. A., Whittaker, A. C., & Allen, P. A. \(2011\). Transformation of tectonic and climatic signals from source to sedimentary archive. \*Nature Geoscience\*, 4\(4\), 231-235.](#)
- [Armitage, J. J., Whittaker, A. C., Zakari, M., & Campforts, B. \(2018\). Numerical modelling of landscape and sediment flux response to precipitation rate change. \*Earth Surface Dynamics\*, 6\(1\), 77-99.](#)
- 395 [Athy, Lawrence Ferdinand. "Density, porosity, and compaction of sedimentary rocks." \*Aapg Bulletin\* 14, no. 1 \(1930\): 1-24.](#)
- [Catuneanu, O. \(2006\). \*Principles of sequence stratigraphy\*\(pp.92-93\). Elsevier.](#)
- [Dalman RA, Weltje GJ. SimClast: An aggregated forward stratigraphic model of continental shelves. \*Computers & geosciences\*. 2012 Jan 1;38\(1\):115-26.](#)
- 400 [Ding X, Salles T, Flament N, et al. Quantitative stratigraphic analysis in a source-to-sink numerical framework. \*Geoscientific Model Development\*, 2019, 12\(6\).](#)
- [Fernandes, Nelson F., and William E. Dietrich. "Hillslope evolution by diffusive processes: The timescale for equilibrium adjustments." \*Water Resources Research\* 33, no. 6 \(1997\): 1307-1318.](#)
- 405 [Guerit, L., Yuan, X. P., Carretier, S., Bonnet, S., Rohais, S., Braun, J., & Rouby, D. \(2019\). Fluvial landscape evolution controlled by the sediment deposition coefficient: Estimation from experimental and natural landscapes. \*Geology\*, 47\(9\), 853-856.](#)
- [Kaufman P, Grotzinger JP, McCormick DS, Franseen EK, Watney WL. Depth-dependent diffusion algorithm for simulation of sedimentation in shallow marine depositional systems. In \*Sedimentary Modeling: Computer Simulations and Methods for Improved Parameter Definition 1991\* \(Vol. 233, pp. 489-508\). \*Kansas Geological Survey Bulletin\*.](#)
- 410 [Li J, Liu P, Zhang J, Sun S, Sun Z, Du D, Zhang M. Base Level Changes based on Basin Filling Modelling: a Case Study from the Paleocene Lishui Sag, East China Sea Basin. \*Petroleum Science\*.<https://doi.org/10.1007/s12182-020-00478-2>](#)
- 415 [Li J, Zhang J, Sun S, Zhang K, Du D, Sun Z, Wang Y, Liu L, Wang G. Sedimentology and mechanism of a lacustrine syn-rift fan delta system: A case study of the Paleogene Gaobei Slope Belt, Bohai Bay Basin, China. \*Marine and Petroleum Geology\*. 2018 Dec 1;98:477-90.](#)
- [Liu P, Yao J, Couples G D, et al. Numerical modelling and analysis of reactive flow and wormhole formation in fractured carbonate rocks. \*Chemical Engineering Science\*, 2017, 172: 143-157.](#)
- 420 [Miall, A. D. \(2016\). \*Stratigraphy: the modern synthesis\*. In \*Stratigraphy: A modern synthesis\* \(pp. 382-386\). Springer, Cham.](#)
- [Moukalled F, Mangani L, Darwish M. \*The finite volume method in computational fluid dynamics\*. Berlin, Germany.: Springer; 2016.](#)
- 425 [Muto T, Steel RJ. Role of autoretreat and A/S changes in the understanding of deltaic shoreline trajectory: a semi - quantitative approach. \*Basin Research\*. 2002 Sep 1;14\(3\):303-18.](#)
- [Nash DB. Morphologic dating of degraded normal fault scarps. \*The Journal of Geology\*. 1980 May 1;88\(3\):353-60.](#)
- [Paola C. Quantitative models of sedimentary basin filling. \*Sedimentology\*. 2000 Feb;47:121-78.](#)
- 430 [Pelletier, Jon. "Fundamental Principles and Techniques of Landscape Evolution Modeling." In \*Treatise on Geomorphology\*, pp. 29-43. Elsevier Inc., 2013.](#)
- [Rivenaes JC. Application of a dual - lithology, depth - dependent diffusion equation in](#)

[stratigraphic simulation. Basin Research. 1992 Jun 1;4\(2\):133-46.](#)

[Rivenaes JC. Impact of sediment transport efficiency on large - scale sequence architecture: results from stratigraphic computer simulation. Basin Research. 1997 Jun;9\(2\):91-105.](#)

435 [Sclater JG, Christie PA. Continental stretching: An explanation of the post - mid - Cretaceous subsidence of the central North Sea basin. Journal of Geophysical Research: Solid Earth. 1980 Jul 10;85\(B7\):3711-39.](#)

[Syvitski JP, Hutton EW. 2d sedflux 1.0 c:: an advanced process-response numerical model for the fill of marine sedimentary basins. Computers & Geosciences. 2001 Jul 1;27\(6\):731-53.](#)

440 [Versteeg HK, Malalasekera W. An introduction to computational fluid dynamics: the finite volume method. Pearson education; 2007.](#)

[Yuan XP, Braun J, Guerit L, Simon B, Bovy B, Rouby D, Robin C, Jiao R. Linking continental erosion to marine sediment transport and deposition: A new implicit and O \(N\) method for inverse analysis. Earth and Planetary Science Letters. 2019 Oct 15;524:115728.](#)

445 [Zhang J, Sylvester Z, Covault J. How do basin margins record long-term tectonic and climatic changes?\[J\]. Geology, 2020.](#)



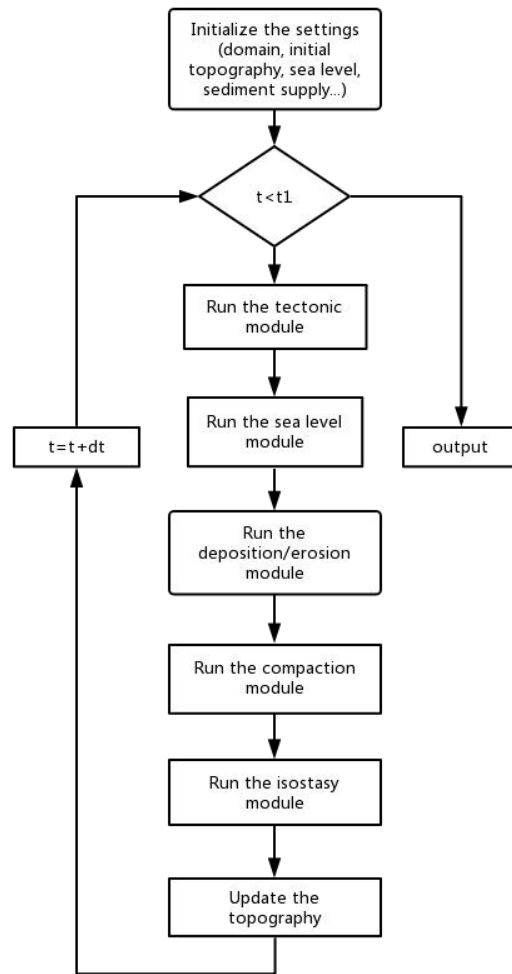
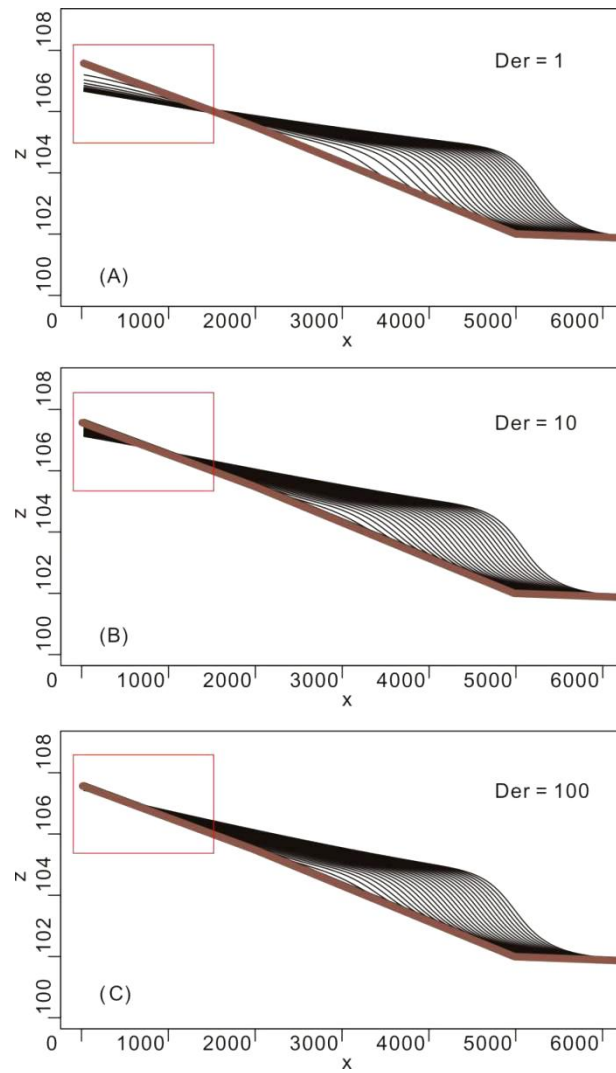


Fig. 1 Flowchart of the algorithms in Sedapp



450 Fig. 2 Dip direction section with different Der values (Der = 1, Der = 10, Der = 100 respectively).

Erosion will be switched off if Der is large enough.

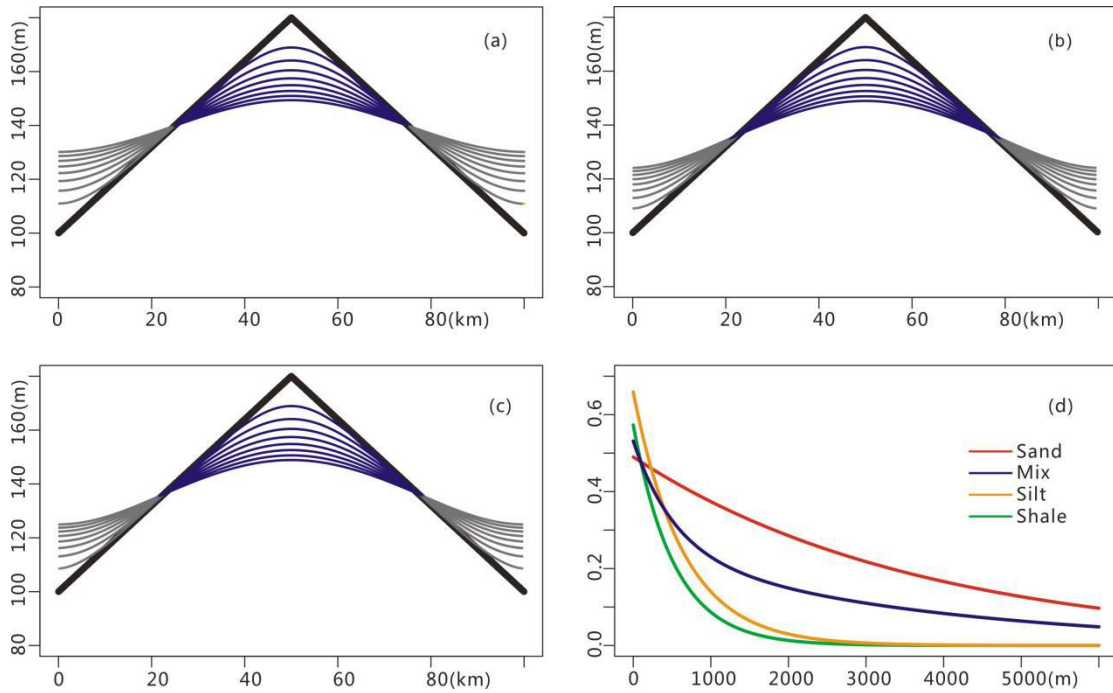


Fig. 3 Customized compaction and the porosity curves. a) the x-z plot with original

depth-porosity scale; b) the x-z plot with magnified depth-porosity scale (x100) to enhance compaction;

455

c) the x-z plot with magnified depth-porosity scale (x1000) to enhance compaction; d) Depth-porosity

curves used in the compaction module (the mix indicates mixed 50%-50% sand and shale. Details see

Athy, 1930; Sclater and Christie 1980)

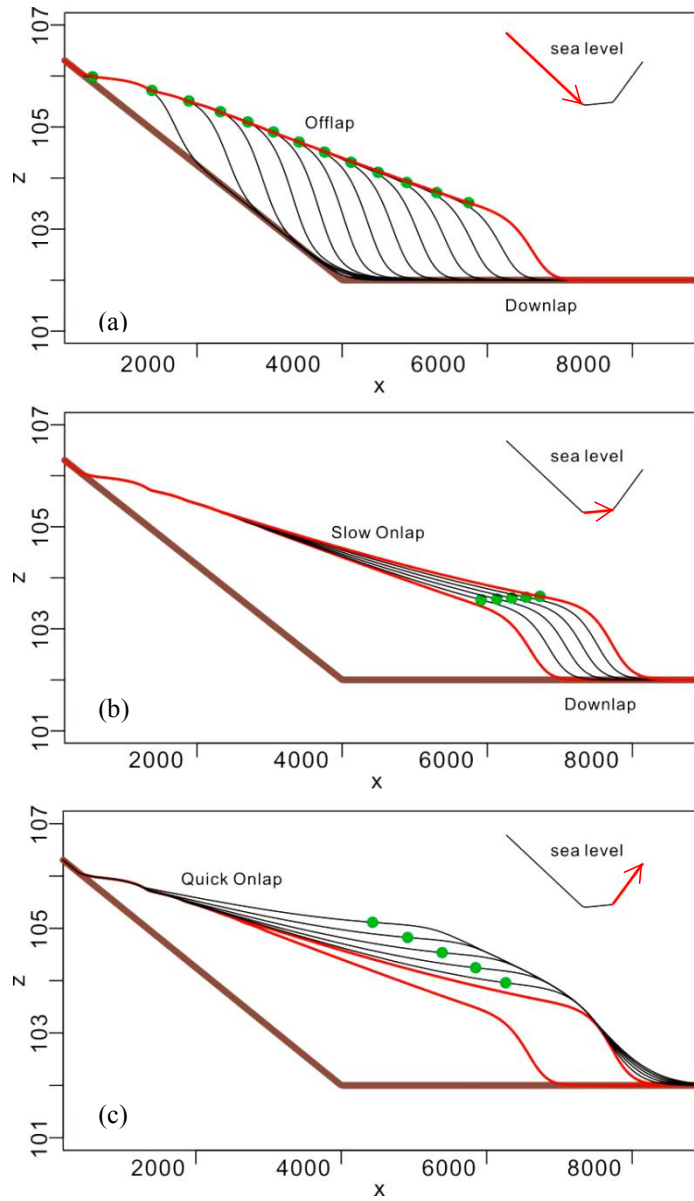
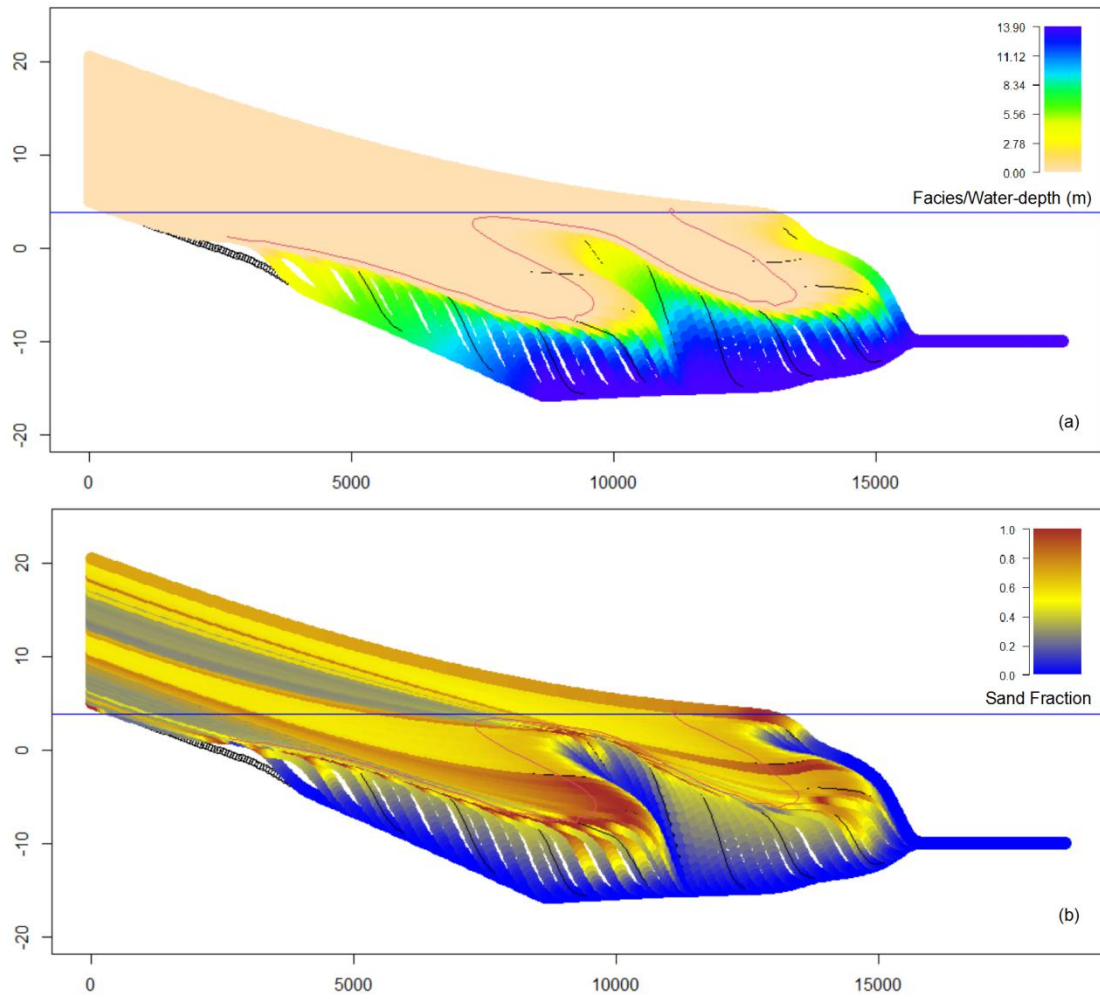
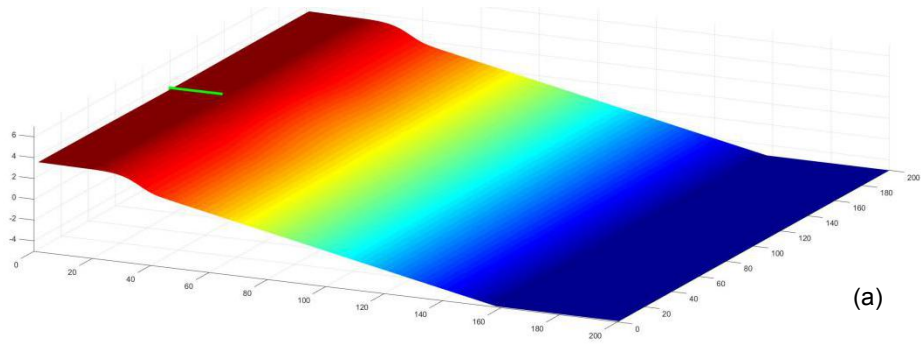


Fig. 4 Typical stacking patterns acquired through different sea level change rates

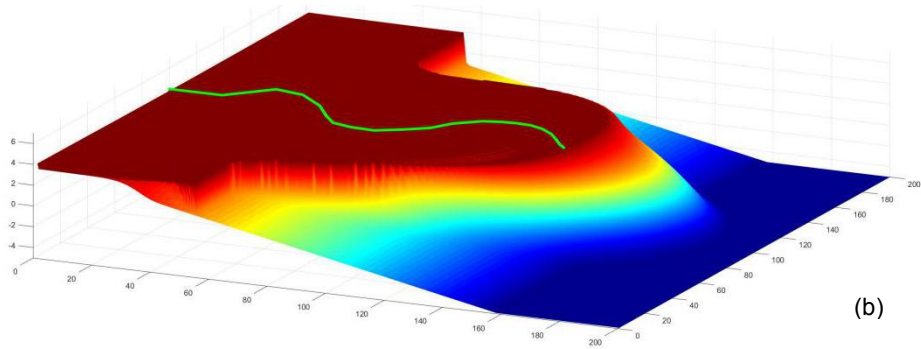


460

Fig. 5 Simulated stratigraphy under two full sea level cycles. A) facies section and B) lithological section.



(a)



(b)

465

Fig. 6 The initial topography and the simulated results of Model 1. (a): the initial topography; (b): the topography at  $t=10$  Ma.

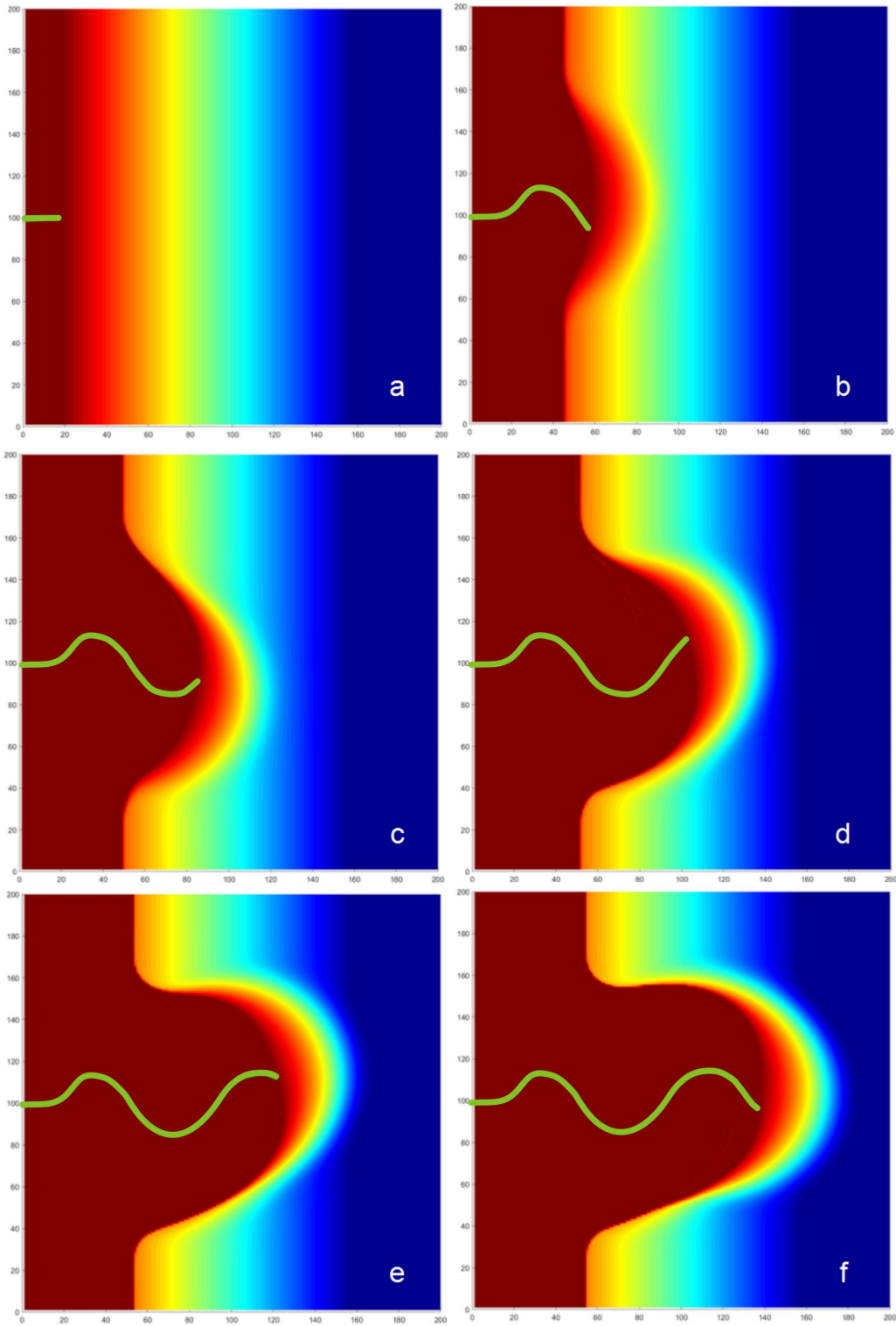


Fig. 7 Plane view of Model 1 results. (a):  $t=0\text{Ma}$ ; (b):  $t=2\text{Ma}$ ; (c):  $t=4\text{Ma}$ ; (d):  $t=6\text{Ma}$ ; (e)  $t=8\text{Ma}$ ;  
 (f)  $t=10\text{Ma}$ .

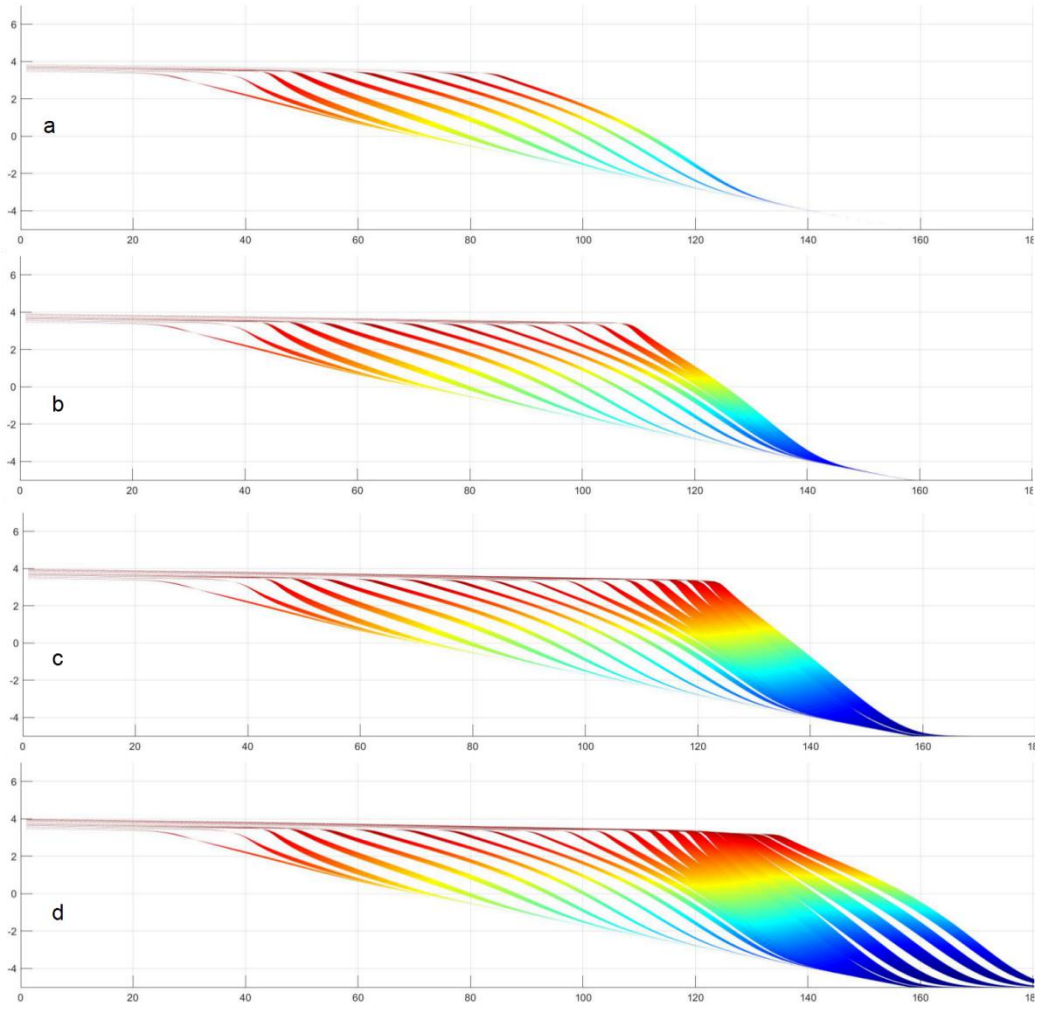


Fig. 8 Cross section at  $x=75\text{m}$ . (a):  $t=4\text{Ma}$ ; (b):  $t=6\text{Ma}$ ; (c):  $t=8\text{Ma}$ ; (d)  $t=10\text{Ma}$ .



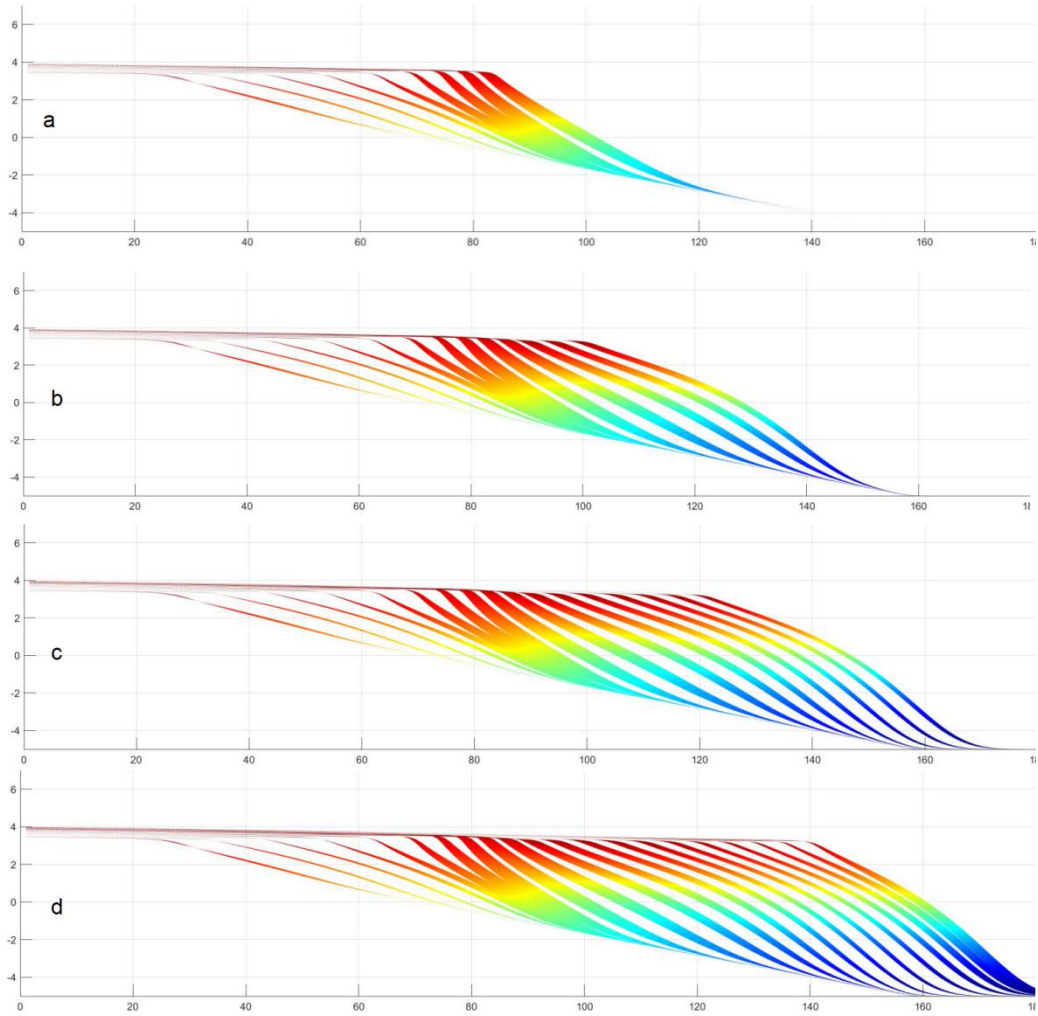
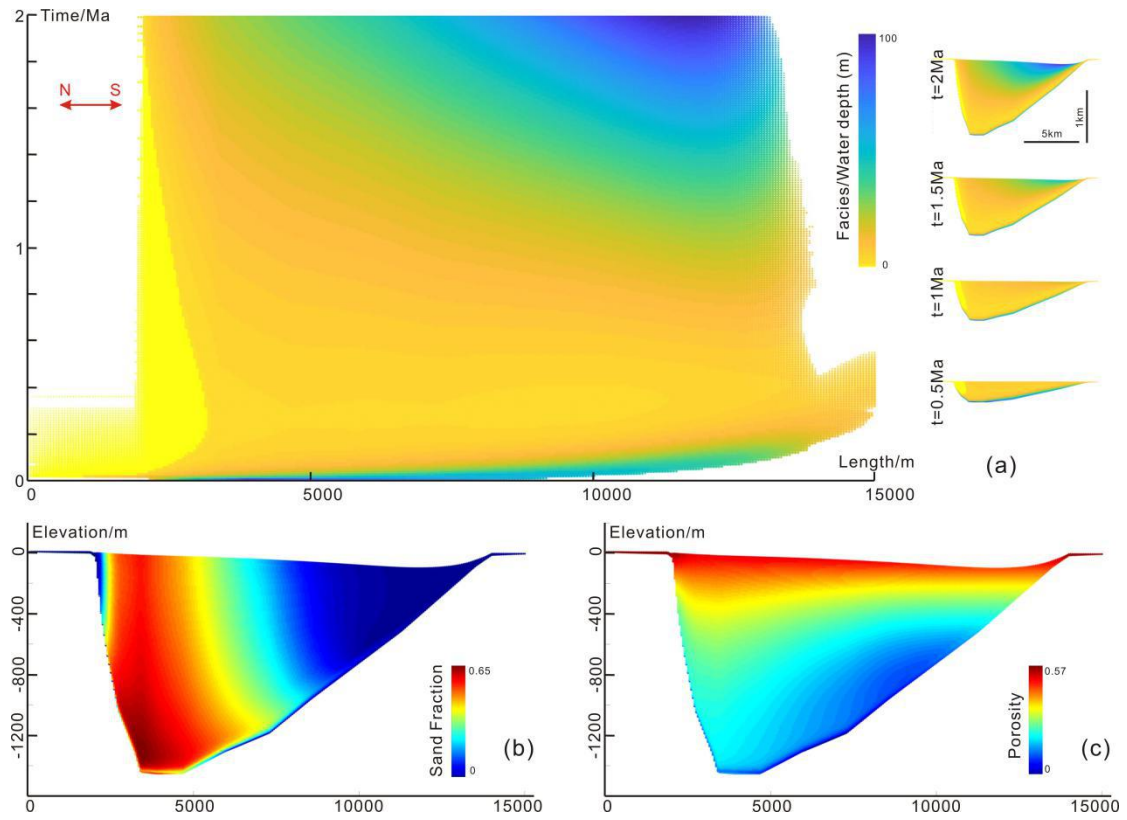


Fig. 9 Cross section at  $x=125m$ . (a):  $t=4Ma$ ; (b):  $t=6 Ma$ ; (c):  $t=8Ma$ ; (d)  $t=10Ma$ .

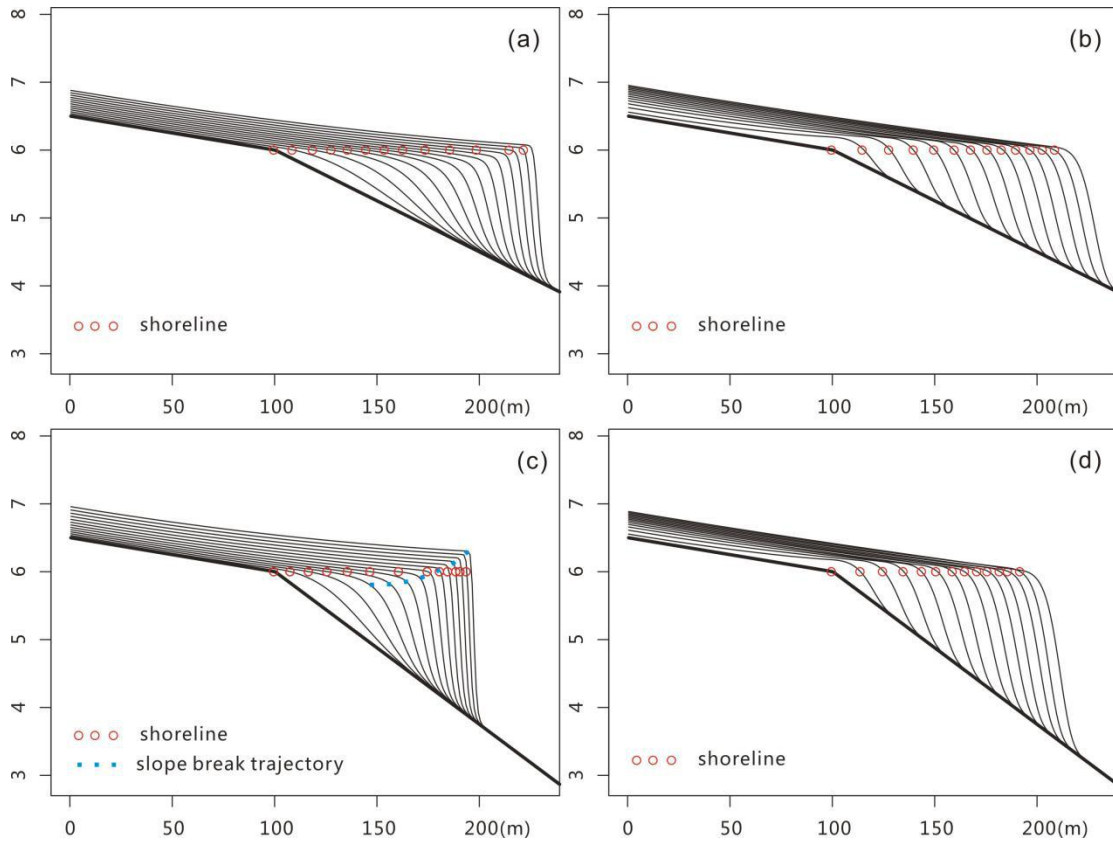
475



Fig. 10 Horton River Delta in Canada (a) and Ebro Delta in Mediterranean Sea (b) (taken from © Google Maps)



480 Fig. 11 Simulation results of Gaobei Slope Belt during the study interval. a) Sedapp results of facies in the time domain (Wheeler diagram) and depth domain at different times; b) Sedapp results of sand fraction in the depth domain. c) Sedapp results of porosity in the depth domain



485

Fig. 12 The differences between two algorithms. a) Clinofoms of gentle slope created in water depth models; b) Clinofoms of gentle slope created in Sedapp; a) Clinofoms of steep slope created in water depth models; b) Clinofoms of steep slope created in Sedapp.

Tab. 1 Main simulation parameters of Model1 (see 2.1 above for meanings of the notations)

Parameter	Value
$\alpha$	1000
$\beta$	500
$\eta$	2
$\alpha_{wd}$	10000
$\beta_{wd}$	0.16
$\eta_{wd}$	1
$\varepsilon$	0
$Der$	1

490